

## 3D-QSAR, molecular docking, and molecular dynamic simulations for prediction of new Hsp90 inhibitors based on isoxazole scaffold

Maryam Abbasi, Hojjat Sadeghi-Aliabadi & Massoud Amanlou

To cite this article: Maryam Abbasi, Hojjat Sadeghi-Aliabadi & Massoud Amanlou (2018) 3D-QSAR, molecular docking, and molecular dynamic simulations for prediction of new Hsp90 inhibitors based on isoxazole scaffold, Journal of Biomolecular Structure and Dynamics, 36:6, 1463-1478, DOI: [10.1080/07391102.2017.1326319](https://doi.org/10.1080/07391102.2017.1326319)

To link to this article: <https://doi.org/10.1080/07391102.2017.1326319>



Accepted author version posted online: 09 May 2017.  
Published online: 24 May 2017.



Submit your article to this journal [↗](#)



Article views: 119



View Crossmark data [↗](#)



Citing articles: 1 View citing articles [↗](#)



## 3D-QSAR, molecular docking, and molecular dynamic simulations for prediction of new Hsp90 inhibitors based on isoxazole scaffold

Maryam Abbasi<sup>a</sup>, Hojjat Sadeghi-Aliabadi<sup>a</sup> and Massoud Amanlou<sup>b\*</sup>

<sup>a</sup>Faculty of Pharmacy, Department of Medicinal Chemistry, Isfahan University of Medical Sciences, 81746-73461 Isfahan, Iran;

<sup>b</sup>Faculty of Pharmacy, Department of Medicinal Chemistry, Drug Design and Development Research Center, Tehran University of Medical Sciences, Tehran, Iran

Communicated by Ramaswamy H. Sarma.

(Received 11 December 2016; accepted 27 April 2017)

Heat shock protein 90 (Hsp90), as a molecular chaperone, play a crucial role in folding and proper function of many proteins. Hsp90 inhibitors containing isoxazole scaffold are currently being used in the treatment of cancer as tumor suppressers. Here in the present studies, new compounds based on isoxazole scaffold were predicted using a combination of molecular modeling techniques including three-dimensional quantitative structure–activity relationship (3D-QSAR), molecular docking and molecular dynamic (MD) simulations. Comparative molecular field analysis (CoMFA) and comparative molecular similarity indices analysis (CoMSIA) were also done. The steric and electrostatic contour map of CoMFA and CoMSIA were created. Hydrophobic, hydrogen bond donor and acceptor of CoMSIA model also were generated, and new compounds were predicted by CoMFA and CoMSIA contour maps. To investigate the binding modes of the predicted compounds in the active site of Hsp90, a molecular docking simulation was carried out. MD simulations were also conducted to evaluate the obtained results on the best predicted compound and the best reported Hsp90 inhibitors in the 3D-QSAR model. Findings indicate that the predicted ligands were stable in the active site of Hsp90.

**Keywords:** Hsp90; isoxazole; 3D-QSAR; CoMFA; CoMSIA; molecular dynamic simulations

### Introduction

Heat shock proteins (Hsps) are a group of evolutionarily conserved proteins that play crucial roles in maintaining cell functions. Among these proteins, Hsp90 is a molecular chaperone protein that is relatively unique (Chen et al., 2014; Sun et al., 2015). Hsp90 plays a vital role in maintaining the conformation, stability, and function of the so-called ‘client’ proteins (Baruchello et al., 2014). In normal cells, Hsp90 constitutes about 1–2% of the total proteins, but it may increase up to 4–6% under stressful conditions (Sun et al., 2015). The homodimer Hsp90 contains three domains: the N-terminal domain, the middle domain, and the C-terminal domain. The Hsp90 function is related to its capability to bind and hydrolyze ATP at the N-terminal domain. First, client protein and co-chaperones bind to the middle domain of Hsp90 in the open state of protein and then ATP binds to N-terminal and Hsp90 is closed. Finally, ATP is hydrolyzed, the complex is altered and the client protein is folded (McLaughlin et al., 2006). Some of the client proteins of Hsp90 significantly contribute to oncogenic cell growth. The competitive inhibition of the ATPase activity of Hsp90 disturbs co-chaperone and client protein complexes, leading to destabilization and degradation of client proteins. Hence,

Hsp90 inhibitors are an attractive therapeutic target for cancer therapy (Wandinger, Richter, & Buchner, 2008).

Hsp90 inhibitors are classified into natural and synthetic inhibitors that are shown in Figure 1. Geldanamycin (GM) and then its derivatives including 17-AAG and 17-DMAG are introduced as first group of natural Hsp90 inhibitors that are shown in Figure 1. Radicol, also known as monorden, with a resorcinol backbone is another natural Hsp90 inhibitor (Sharma, Agatsuma, & Nakano, 1998). The first synthetic inhibitor of Hsp90, PU3, and one of its derivatives (CNF-2024/BI IB021) entered clinical trial in 2005 (Porter, Fritz, & Depew, 2010). Compounds with isoxazole scaffold also nominated as potent Hsp90 inhibitors (NVP-AUY922, Luminespib) (Baruchello et al., 2011; Sharp et al., 2007).

To design new inhibitors, theoretical studies are substantially important in expediting and saving resources. There are several computational methods that simplify the drug discovery process. The quantitative structure–activity relationship (QSAR), a ligand-based drug design method, is a mathematical equation which produces a relationship between chemical structures and their biological activities (Abbasi, Ramezani, Elyasi, Sadeghi-Aliabadi, & Amanlou, 2015). Decreasing toxicity and

\*Corresponding author. Email: [amanlou@tums.ac.ir](mailto:amanlou@tums.ac.ir)

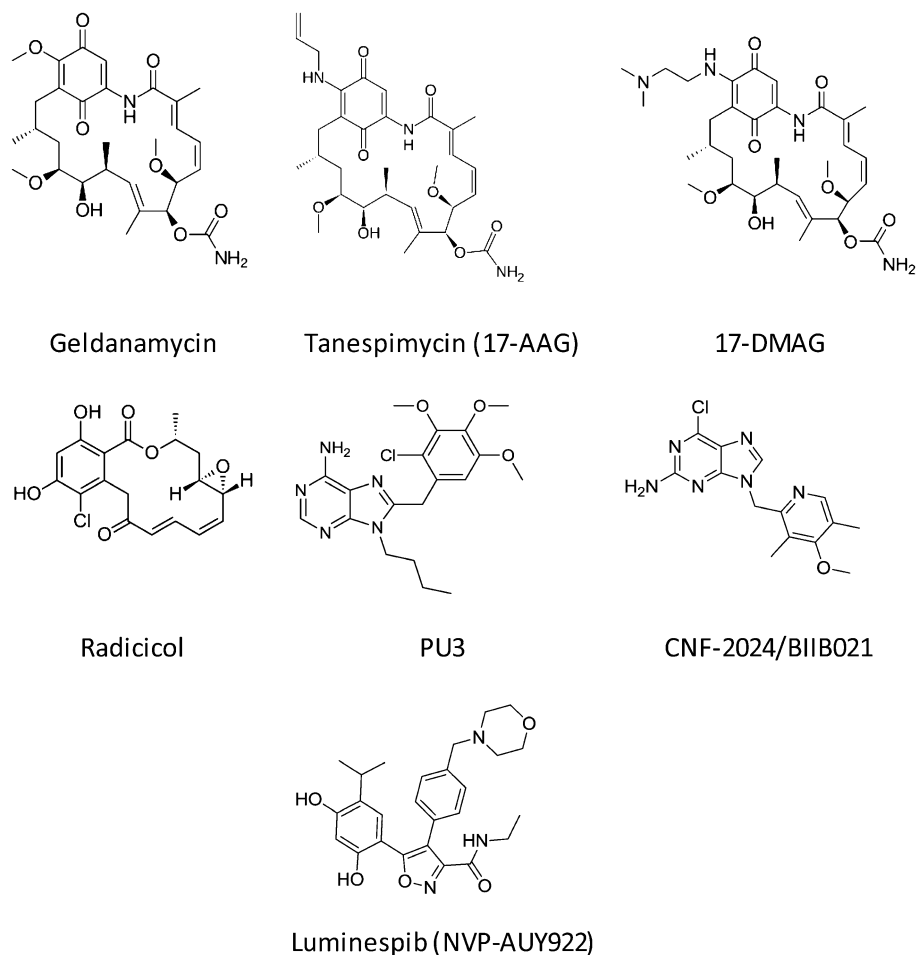


Figure 1. Chemical structures of well-known Hsp90 Inhibitors.

improving pharmacological activity of designed compounds will be the next aim of QSAR studies. However, in QSAR techniques, limited utility for designing functional new molecules exist because of the lack of the three-dimensional (3D) structures of the molecules. Consequently, 3D-QSAR has appeared as a useful tool that uses the 3D attributes of the ligands to predict their biological activity by applying strong chemometric tools (Athar, Lone, Khedkar, & Jha, 2016; Roy, Kar, & Das, 2015; Tripuraneni & Azam, 2016; Zhou et al., 2016). The most popular 3D-QSAR studies based on the spatial alignment of molecules are comparative molecular field analysis (CoMFA) and comparative molecular similarity indices analysis (CoMSIA). The CoMFA analysis is ligand-based method expanded by Cramer et al. which assists in building the quantitative relationship of molecular structures. The CoMSIA analysis is a linear 3D-QSAR method that is an improved version of CoMFA (Cramer, Bunce, Patterson, & Frank, 1988; Klebe, Abraham, & Mietzner, 1994).

On the other hand, molecular docking and molecular dynamics (MD) simulation, which are structure-based drug design methods, are used to predict the conceivable orientation of a ligand in the active site of a receptor as well as conformational changes of molecules (Ma et al., 2015). Therefore, a combined 3D-QSAR, molecular docking, and MD simulation study can provide to profound insights into ligand-receptor interactions and prediction of new compounds.

In this study, 3D-QSAR models were generated for 81 compounds, synthesized during 2012 and 2015, and some new compounds were predicted (Bargiotti et al., 2012; Baruchello et al., 2014; Chen et al., 2014; Musso, Cincinelli, Giannini, Manetti, & Dallavalle, 2015; Sun et al., 2015). Here the interactions between the new predicted ligands and Hsp90 were investigated by molecular docking and MD simulation, the latter was done on one of the best new ligands in terms of energy and interaction to certify the stability of the new predicted ligand in the dynamic environment.

## Methodology

### Data-set and alignment

In the present study, 3D-QSAR analyses were performed using the SYBYL-X 2.0 package (Tripos Inc. St. Louis, USA). Several series of isoxazole derivatives as potent Hsp90 inhibitors were synthesized by five different teams during 2012 and 2015 (Bargiotti et al., 2012; Baruchello et al., 2014; Chen et al., 2014; Musso et al., 2015; Sun et al., 2015). Among all reported compounds, 81 were chosen (Table 1). All 81 compounds were optimized using Tripos force field and Gasteiger-Huckel charges with NB cutoff of 8.00 and dielectric constant of 1.00. The structural energy minimization was terminated using Powell gradient algorithm with a convergence criterion of 0.005 kcal/(mol Å) and a maximum of 10,000 iterations.

Among all 81 compounds, 54 were chosen as a training set and 27 were chosen as a test set. Binding affinity for all of the synthesized compounds is reported by a fluorescence polarization assay and summarized in Table 2.

### Molecular docking

To find the predicted compounds' interactions and binding energy with Hsp90, a molecular docking was done by AutoDock 4.2 program (Morris et al., 2009). Among the experimental X-ray structures of human Hsp90, the crystallographic structure with a PDB entry code of 3OWD (1.63 Å resolution) was elected (Bruncko et al., 2010).

For protein preparation, the co-crystallized ligand and water molecules, except for the water molecules that were important in the interaction between the ligand and protein, were eliminated. By AutoDockTools 1.5.6 package (Morris et al., 2009), all missing hydrogens were added. After calculating Kollman atom charges, non-polar hydrogens were merged and the file was saved as pdbqt. A grid box was made with a grid point spacing of 0.375 Å and 90 × 90 × 90 points, which included not only the active site of the protein but also significant regions of the surrounding surface. Before calculating the grid maps by AutoGrid 4.2 (Azizian, Bahrami, Pasalar, & Amanlou, 2010), water molecule parameters were added to AD4-bound and AD4-parameter files.

After creation of ligand, the 3D structures of all of the compounds were depicted in Marvin Sketch Ver. 5.7, ChemAxon (Cosconati et al., 2010). The partial charges of atoms were computed using the Gasteiger-Marsili procedure, and non-polar hydrogens of the compounds were merged (Morris et al., 1998).

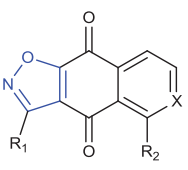
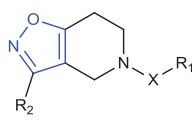
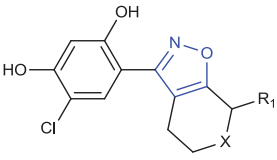
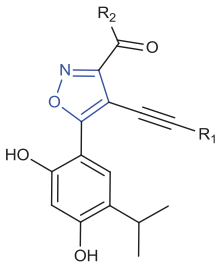
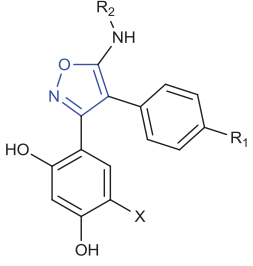
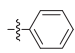
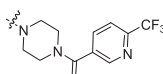
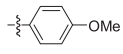
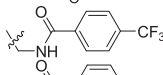
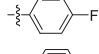
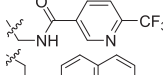
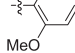
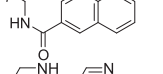
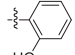
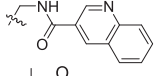
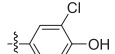
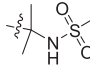
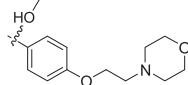
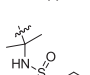
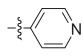
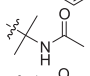
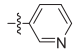
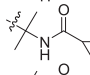
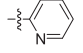
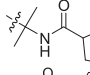
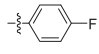
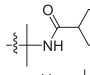
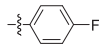
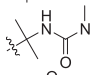
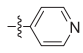
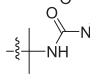
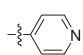
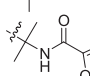
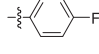
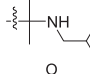
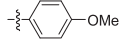
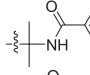
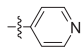
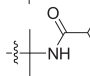
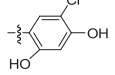
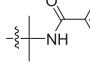
The Lamarckian genetic algorithm approach was chosen for the global optimum binding position. Docking calculation parameters were specified as follows: the

number of Lamarckian job = 50, initial population = 150, maximum number of energy evaluation =  $25 \times 10^5$ , and the default values of other parameters were kept unchanged. The docking parameter file (.dpf) was built. The docking procedure was performed by AutoDock 4.2 and the .dlg file was produced. All of the runs were ranked by the maximum number of clusters and the lowest binding energy, and .dlg files were analyzed to achieve the best conformation of the ligand with key residues in the active site of the protein by Accelrys Discovery Studio 2.5 package (<http://accelrys.com/products/collaborative-science/biovia-discovery-studio/>) and PyMOL software (Makarewicz & Kaźmierkiewicz, 2013; PyMOL, 2010).

### MD simulation

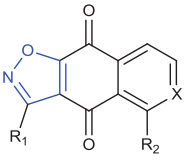
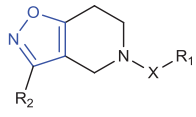
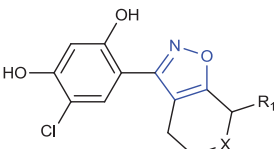
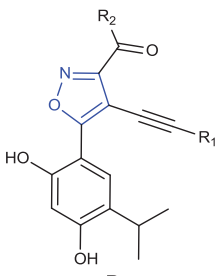
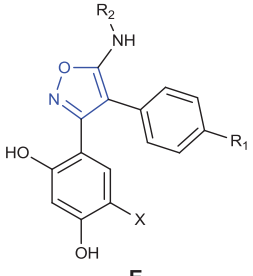
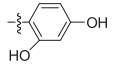
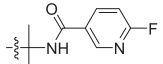
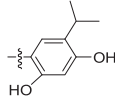
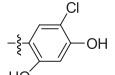
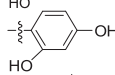
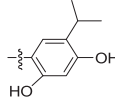
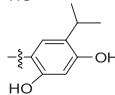
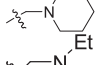
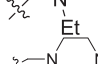
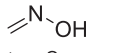
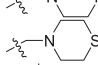
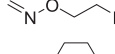
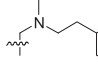
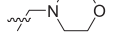
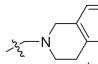

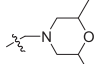
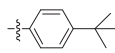
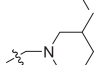
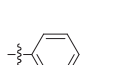
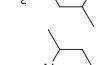
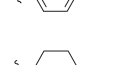
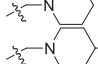
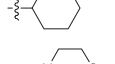
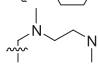
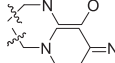
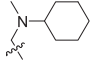
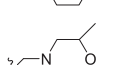
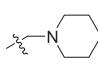
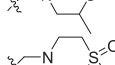
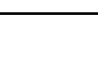
MD simulation was performed with the GROMACS 5.0.5 package (Abraham et al., 2015). The topology parameters of the best predicted ligand in terms of the energy and interaction between the ligand and protein were obtained by the PRODRG web server (Schüttelkopf & van Aalten, 2004). The obtained charges by PRODRG web server were edited by Gaussian98 program (Frisch, 1998; Frisch et al., 2004). pKa for residues of protein were calculated by the PROPKA 3.1 web server to characterize which residue was more likely to accept non-standard ionization states (Søndergaard, Olsson, Rostkowski, & Jensen, 2011). The main crystallographic water molecules in the active site were kept (Abbasi, Sadeghi-Aliabadi, Hassanzadeh, & Amanlou, 2015). The GROMOS96 54a7 force field (Schmid et al., 2011) and the simple point charges water model were used to create protein topology parameters. The ligand and protein complex was dunked in a dodecahedron box with a minimum distance of 1 nm between the protein surface and the box boundary, containing about 8250 solvent molecules. By replacing solvent water molecules with 4 Na<sup>+</sup> the net charge of the system was neutralized. The energy minimization was done to release spatial clashes of the complex in two steps. First, only water molecules were minimized using 10,000 steepest descents steps, while the other atoms were kept fixed at their initial configuration. After that, the whole system was minimized. To equilibrate the system at a constant temperature of 300 K, the NVT step was performed with a 500 ps MD run. After stabilization of the temperature by the V-Rescale algorithm, an NPT ensemble was performed with a time duration of 1 ns. This was followed by MD production run at 1 bar pressure and 100 K, 200 K, and 300 K temperatures for 1, 2, and 50 ns, respectively. Long-range electrostatic interactions were calculated with the Particle Mesh Ewald method. The linear constraint (LINCS) algorithm was applied for covalent bond constraints. Structure visualization was performed using

Table 1. The molecular structures of studied compounds.

																			
Comp.	R <sub>1</sub>	R <sub>2</sub>	X	Comp.	R <sub>1</sub>	R <sub>2</sub>	X												
<b>3a (A)</b>		H	C	<b>19g (D)</b>		NHCH <sub>2</sub> CH <sub>3</sub>	–												
<b>3b (A)</b>		H	C	<b>19h (D)</b>		NHCH <sub>2</sub> CH <sub>3</sub>	–												
<b>3d (A)</b>		H	C	<b>19i (D)</b>		NHCH <sub>2</sub> CH <sub>3</sub>	–												
<b>3e (A)</b>		H	C	<b>19j (D)</b>		NHCH <sub>2</sub> CH <sub>3</sub>	–												
<b>3f (A)</b>		H	C	<b>19k (D)</b>		NHCH <sub>2</sub> CH <sub>3</sub>	–												
<b>3i (A)</b>		H	C	<b>20a (D)</b>		NHCH <sub>2</sub> CH <sub>3</sub>	–												
<b>3k (A)</b>		H	C	<b>20b (D)</b>		NHCH <sub>2</sub> CH <sub>3</sub>	–												
<b>3n (A)</b>		H	C	<b>20c (D)</b>		NHCH <sub>2</sub> CH <sub>3</sub>	–												
<b>3o (A)</b>		H	C	<b>20d (D)</b>		NHCH <sub>2</sub> CH <sub>3</sub>	–												
<b>3p (A)</b>		H	C	<b>20e (D)</b>		NHCH <sub>2</sub> CH <sub>3</sub>	–												
<b>6a (A)</b>		OAc	C	<b>20f (D)</b>		NHCH <sub>2</sub> CH <sub>3</sub>	–												
<b>6b (A)</b>		H	C	<b>20g (D)</b>		NHCH <sub>2</sub> CH <sub>3</sub>	–												
<b>6c (A)</b>		Me	C	<b>20h (D)</b>		NHCH <sub>2</sub> CH <sub>3</sub>	–												
<b>6d (A)</b>		OAc	C	<b>20i (D)</b>		NHCH <sub>2</sub> CH <sub>3</sub>	–												
<b>10a (A)</b>		H	N	<b>20j (D)</b>		NHCH <sub>2</sub> CH <sub>3</sub>	–												
<b>10b (A)</b>		H	N	<b>20k (D)</b>		NHCH <sub>2</sub> CH <sub>3</sub>	–												
<b>10d (A)</b>		H	N	<b>20m (D)</b>		NHCH <sub>2</sub> CH <sub>3</sub>	–												
<b>13 (B)</b>		COOEt	CO	<b>20p (D)</b>		NHCH <sub>2</sub> CH <sub>3</sub>	–												

(Continued)

Table 1. (Continued).

																			
Comp.	R <sub>1</sub>	R <sub>2</sub>	X	Comp.	R <sub>1</sub>	R <sub>2</sub>	X												
<b>14 (B)</b>		COOEt	CO	<b>20q (D)</b>		NHCH <sub>2</sub> CH <sub>3</sub>	–												
<b>15 (B)</b>		COOEt	CO	<b>23 (E)</b>	OMe	H	Cl												
<b>17 (B)</b>		CONHEt	CO	<b>24 (E)</b>	OMe	COMe	Cl												
<b>18 (B)</b>		CONHEt	CO	<b>32 (E)</b>	OMe	CO-cycloPn	Cl												
<b>25 (B)</b>		CONH-(CH <sub>2</sub> ) <sub>2-4</sub> -morpholine	CO	<b>34 (E)</b>	OMe	CO-cycloHp	Cl												
<b>26 (B)</b>		CONH-cyclopentyl	CO	<b>57 (E)</b>	OMe	COMe	H												
<b>9a (C)</b>	=O	–	NMe	<b>59 (E)</b>	OMe	COMe	t-Bu												
<b>9b (C)</b>	=O	–	NH	<b>60 (E)</b>	OMe	CO-cycloPr	i-Pr												
<b>13 (C)</b>	=O	–	C	<b>94 (E)</b>		CO-cycloPr	i-Pr												
<b>14 (C)</b>	OH	–	C	<b>95 (E)</b>		CO-cycloPr	i-Pr												
<b>15 (C)</b>		–	C	<b>96 (E)</b>		CO-cycloPr	i-Pr												
<b>16 (C)</b>		–	C	<b>97 (E)</b>		CO-cycloPr	i-Pr												
<b>14b (D)</b>		NHCH(CH <sub>2</sub> ) <sub>2</sub>	–	<b>99 (E)</b>		CO-cycloPr	i-Pr												
<b>15a (D)</b>		NHCH(CH <sub>2</sub> ) <sub>2</sub>	–	<b>100 (E)</b>		CO-cycloPr	i-Pr												
<b>18a (D)</b>		NHCH <sub>2</sub> CH <sub>3</sub>	–	<b>101 (E)</b>		CO-cycloPr	i-Pr												
<b>18b (D)</b>		NHCH <sub>2</sub> CH <sub>3</sub>	–	<b>102 (E)</b>		CO-cycloPr	i-Pr												
<b>18c (D)</b>		NHCH <sub>2</sub> CH <sub>3</sub>	–	<b>103 (E)</b>		CO-cycloPr	i-Pr												
<b>19a (D)</b>		NHCH <sub>2</sub> CH <sub>3</sub>	–	<b>104 (E)</b>		CO-cycloPr	i-Pr												
<b>19b (D)</b>		NHCH <sub>2</sub> CH <sub>3</sub>	–	<b>105 (E)</b>		CO-cycloPr	i-Pr												
<b>19c (D)</b>		NHCH <sub>2</sub> CH <sub>3</sub>	–	<b>106 (E)</b>		CO-cycloPr	i-Pr												
<b>19d (D)</b>		NHCH <sub>2</sub> CH <sub>3</sub>	–	<b>107 (E)</b>		CO-cycloPr	i-Pr												

(Continued)

Table 1. (Continued).

Comp.	R <sub>1</sub>	R <sub>2</sub>	X	Comp.	R <sub>1</sub>	R <sub>2</sub>	X	Comp.	R <sub>1</sub>	R <sub>2</sub>	X	Comp.	R <sub>1</sub>	R <sub>2</sub>	X				
<b>19e (D)</b>		NHCH <sub>2</sub> CH <sub>3</sub>	–	<b>108 (E)</b>		CO-cycloPr	i-Pr												
<b>19f (D)</b>		NHCH <sub>2</sub> CH <sub>3</sub>	–																

Table 2. Actual and predicted pIC<sub>50</sub> (μM) values of CoMFA and CoMSIA.

Comp.	Actual pIC <sub>50</sub> (μM)	Predicted CoMFA	Residual	Predicted CoMSIA	Residual	Comp.	Actual pIC <sub>50</sub> (μM)	Predicted CoMFA	Residual	Predicted CoMSIA	Residual
<b>3a (A)</b>	5.105	5.569	-0.464	5.726	-0.621	<b>19g (D)</b>	7.347	6.979	0.368	7.619	-0.272
<b>3b (A)</b>	5.234	5.308	-0.074	5.670	-0.436	<b>19h (D)</b>	6.684	6.673	0.011	6.720	-0.036
<b>3d (A)</b>	3.699	5.724	-2.025	5.496	-1.797	<b>19i (D)</b>	7.180	6.755	0.425	6.867	0.313
<b>3e (A)</b>	3.699	5.413	-1.714	4.837	-1.138	<b>19j (D)</b>	6.263	6.374	-0.111	6.254	0.009
<b>3f (A)</b>	5.810	5.805	0.005	5.700	0.110	<b>19k (D)</b>	5.780	6.467	-0.687	6.251	-0.471
<b>3i (A)</b>	5.377	6.098	-0.721	5.757	-0.380	<b>20a (D)</b>	6.921	7.135	-0.214	6.976	-0.055
<b>3k (A)</b>	5.921	5.385	0.536	5.808	0.113	<b>20b (D)</b>	7.108	6.960	0.148	6.529	0.579
<b>3n (A)</b>	6.409	5.828	0.581	6.126	0.283	<b>20c (D)</b>	7.301	7.129	0.172	6.962	0.339
<b>3o (A)</b>	6.268	5.782	0.486	5.942	0.326	<b>20d (D)</b>	6.896	7.009	-0.113	6.868	0.028
<b>3p (A)</b>	5.975	5.790	0.185	5.839	0.136	<b>20e (D)</b>	6.738	6.882	-0.144	6.854	-0.116
<b>6a (A)</b>	5.712	6.063	-0.351	5.919	-0.207	<b>20f (D)</b>	7.004	6.790	0.214	6.736	0.268
<b>6b (A)</b>	6.538	6.272	0.266	5.773	0.765	<b>20g (D)</b>	6.513	6.897	-0.384	6.448	0.065
<b>6c (A)</b>	5.721	6.073	-0.352	6.316	-0.595	<b>20h (D)</b>	6.327	6.988	-0.661	6.375	-0.048
<b>6d (A)</b>	7.076	6.384	0.692	6.617	0.459	<b>20i (D)</b>	6.967	6.723	0.244	6.613	0.354
<b>10a (A)</b>	5.252	4.972	0.280	5.048	0.204	<b>20j (D)</b>	6.263	6.874	-0.611	6.336	-0.073
<b>10b (A)</b>	5.796	5.317	0.479	5.067	0.729	<b>20k (D)</b>	5.780	6.802	-1.022	6.236	-0.456
<b>10d (A)</b>	6.921	6.079	0.842	6.186	0.735	<b>20m (D)</b>	6.530	6.809	-0.279	6.835	-0.305
<b>13 (B)</b>	6.796	6.221	0.575	6.333	0.463	<b>20p (D)</b>	6.917	6.851	0.066	6.296	0.621
<b>14 (B)</b>	5.409	6.045	-0.636	5.868	-0.459	<b>20q (D)</b>	7.180	6.918	0.262	6.833	0.347
<b>15 (B)</b>	7.000	6.736	0.264	6.922	0.078	<b>23 (E)</b>	7.276	7.283	-0.007	7.384	-0.108
<b>17 (B)</b>	6.959	6.248	0.711	6.622	0.337	<b>24 (E)</b>	7.155	7.102	0.053	7.303	-0.148
<b>18 (B)</b>	5.921	6.116	-0.195	6.157	-0.236	<b>32 (E)</b>	7.056	6.374	0.682	7.057	-0.001
<b>25 (B)</b>	7.268	7.260	0.008	7.076	0.192	<b>34 (E)</b>	6.745	6.567	0.178	7.082	-0.337
<b>26 (B)</b>	7.167	7.051	0.116	6.820	0.347	<b>57 (E)</b>	6.854	6.844	0.010	7.199	-0.345
<b>9a (C)</b>	5.000	5.004	-0.004	4.908	0.092	<b>59 (E)</b>	6.523	6.406	0.117	6.573	-0.050
<b>9b (C)</b>	5.796	5.766	0.030	5.290	0.506	<b>60 (E)</b>	7.638	7.454	0.184	7.558	0.080
<b>13 (C)</b>	5.319	5.108	0.211	5.186	0.133	<b>94 (E)</b>	7.770	7.490	0.280	7.424	0.346
<b>14 (C)</b>	4.585	5.256	-0.671	5.190	-0.605	<b>95 (E)</b>	7.678	7.049	0.629	7.202	0.476
<b>15 (C)</b>	7.000	6.736	0.264	6.922	0.078	<b>96 (E)</b>	7.569	7.583	-0.014	7.540	0.029
<b>16 (C)</b>	5.201	4.868	0.333	4.507	0.694	<b>97 (E)</b>	7.244	7.577	-0.333	7.517	-0.273
<b>14b (D)</b>	6.967	7.093	-0.126	7.155	-0.188	<b>99 (E)</b>	6.854	7.128	-0.274	7.149	-0.295
<b>15a (D)</b>	7.347	7.381	-0.034	7.181	0.166	<b>100 (E)</b>	7.444	7.525	-0.081	7.527	-0.083
<b>18a (D)</b>	6.460	6.974	-0.514	6.637	-0.177	<b>101 (E)</b>	7.538	7.582	-0.044	7.461	0.077
<b>18b (D)</b>	6.903	7.354	-0.451	7.179	-0.276	<b>102 (E)</b>	7.337	7.180	0.157	7.336	0.001
<b>18c (D)</b>	6.818	6.860	-0.042	6.996	-0.178	<b>103 (E)</b>	7.456	7.605	-0.149	7.501	-0.045
<b>19a (D)</b>	7.180	7.086	0.094	7.244	-0.064	<b>104 (E)</b>	7.155	7.199	-0.044	7.335	-0.180
<b>19b (D)</b>	7.319	7.018	0.301	7.564	-0.245	<b>105 (E)</b>	7.260	7.284	-0.024	7.411	-0.151
<b>19c (D)</b>	7.041	6.908	0.133	7.057	-0.016	<b>106 (E)</b>	7.237	7.162	0.075	7.264	-0.027
<b>19d (D)</b>	7.553	7.149	0.404	7.233	0.320	<b>107 (E)</b>	7.357	7.200	0.157	7.345	0.012
<b>19e (D)</b>	6.943	7.013	-0.070	7.107	-0.164	<b>108 (E)</b>	7.523	7.196	0.327	7.404	0.119
<b>19f (D)</b>	6.842	6.819	0.023	6.964	-0.122						

VMD 1.8.6 (Humphrey, Dalke, & Schulten, 1996) and PyMOL softwares.

## Results and discussion

### CoMFA and CoMSIA statistical results

In this study, the compound 94(E) with high potency was elected as a template molecule and the other geometrically optimized molecules were superimposed onto its red atoms by using database alignment in SYBYL (Figure 2).

The partial least squares (PLS) method was applied to quantify the communication between the CoMFA and CoMSIA descriptors and the biological activities (Pourbasheer, Bazl, & Amanlou, 2014). Activities and the residual values of all compounds were calculated by the best model of CoMFA and CoMSIA that are presented in Table 2. The correlation between the predicted activities and experimental activities by CoMFA and CoMSIA models are also shown in Figure 3.

The leave-one-out (LOO) cross-validation method was done, and one compound was deleted from the data-set and its activity was predicted using the model resulting from the rest of the data-set. To evaluate the non-cross-validated model, the squared correlation coefficient ( $r^2$ ) and standard error of estimate (SEE) were calculated. The quality of the model was evaluated by the cross-validated coefficient ( $q^2$ ). Column filtering value of 2.00 kcal/mol was used to speed up the analysis and reduce the noise (Ouyang et al., 2012). Mean absolute error (MAE) was computed between predicted and actual efficacy of molecules using following equation (Chauhan et al., 2014):

$$MAE = \frac{\sum_{i=1}^N |(pIC_{50} \text{ actual} - pIC_{50} \text{ predicted})|}{N}$$

For CoMFA analysis with steric and electrostatic fields, an optimal number of components (ONC),  $q^2$ ,  $r^2$ , MAE, and SEE values were obtained, at 4, 0.553, 0.719, 0.293,

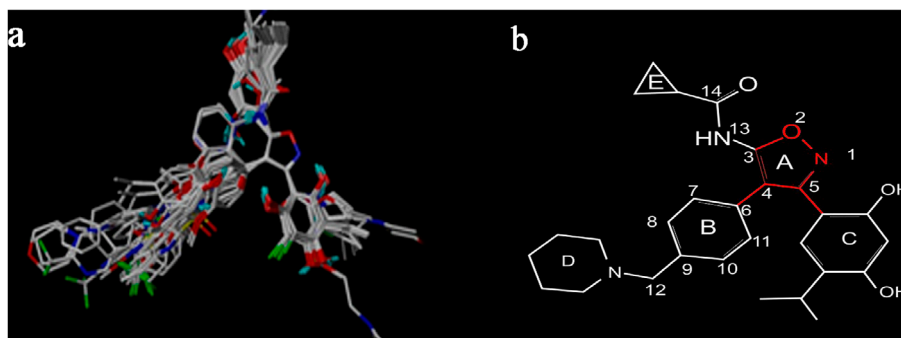


Figure 2. (a) The alignment of all studied compounds. (b) The atoms used to automatically position the compounds by using database alignment (red).

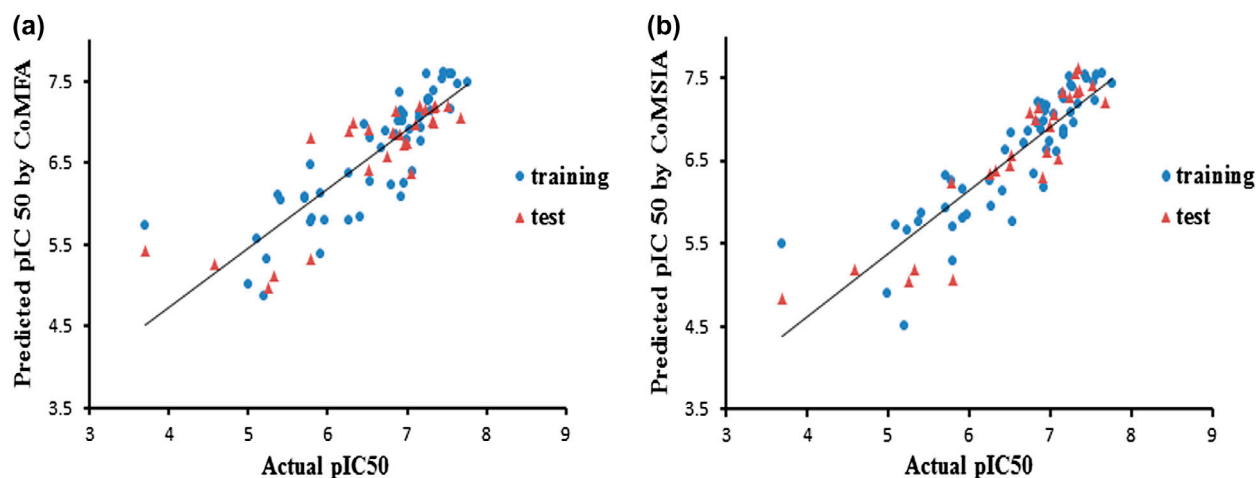


Figure 3. Plots of predicted versus actual  $pIC_{50}$  values for all the molecules; (a) based on CoMFA and (b) based on CoMSIA.



and 0.464, respectively. The steric and electrostatic field contributions to the CoMFA model were 73.93 and 26.07%, respectively. Five descriptor fields of CoMSIA including steric, electrostatic, hydrophobic, donor, and acceptor H-bond were evaluated.  $q^2$ ,  $r^2$ , MAE, and SEE values were calculated as 0.538, 0.765, 0.292, and 0.425, respectively. In CoMFA and CoMSIA analysis,  $q^2$  and  $r^2$  values were higher than 0.5 and 0.6, respectively. All of the 31 possible combination descriptors of CoMSIA were considered since the dependency on the five CoMSIA descriptors could decrease the model's significance (Bringmann & Rummey, 2003). As shown in Figure 4, the donor field presents the highest  $q^2$  value (0.508), so  $q^2$  gave rise when the donor was used with other fields.

The CoMFA and CoMSIA models were validated by the test set. The  $r^2$  values of CoMFA and CoMSIA were calculated 0.653 and 0.823, respectively. Although the CoMFA model yielded good results for the training set ( $r^2 = 0.719$ ), it did not produce good results for the test set ( $r_{\text{test}}^2 = 0.653$ ). As a result, the CoMSIA model is superior to the CoMFA model.

#### Contour maps of CoMFA and CoMSIA

The field influence on the target molecules can be displayed as 3D contour maps. The contour maps were generated employing field type  $\text{StDev} \times \text{Coeff}$  to determine main regions where some changes in CoMFA and CoMSIA fields can influence the biological activity (Yang et al., 2013). To illustrate all contour maps of CoMFA and CoMSIA models, compound 94(E) was chosen as the reference.

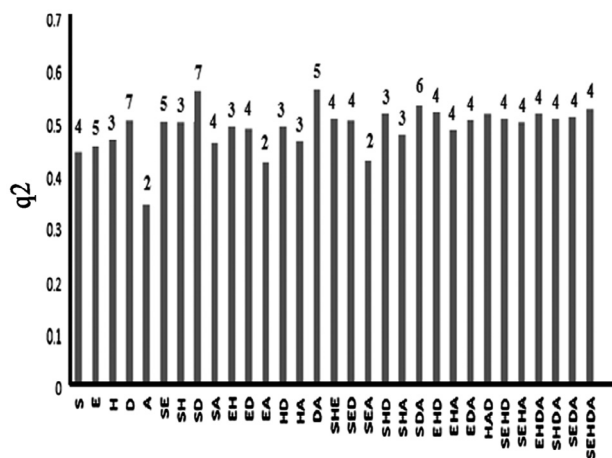


Figure 4. The  $q^2$  values of 31 possible combinations descriptors of CoMSIA (S steric, E electrostatic, H hydrophobic, D/A H-bond donor/acceptor) and their ONC was reported above the bars.

Figure 5(a) and (b) displays the contour plots for the steric and electrostatic fields of the CoMFA and CoMSIA models. The green (80% contribution) and yellow (20% contribution) contours indicate the favorable and unfavorable steric interactions, respectively. One green and two yellow contours are enclosed between B and D rings, suggesting that medium-sized groups are favored in this region. A green contour near ring E indicates that a bulky group is favorable for activity. Whereas a yellow contour map adjacent the resorcinol ring shows that bulky groups are not favored in this region. The CoMFA steric contour maps are in agreement with the experimental data: in most active compounds such as 94(E), 19d(D), 25(B), and 6d(A), a medium-sized group is seen in the region of ring D. However, for the 3d(A) compound as a least active compound, bulky groups were not found in the region of rings B, D, and E, but were observed in unfavorable regions above ring B.

In Figure 5(c) and (d), the blue and red contours illustrate the favorable and unfavorable electrostatic interaction in CoMFA and CoMSIA models, respectively. In CoMFA contour map, presence of the blue contour near the OH groups in the resorcinol ring and also near the N atom of the isoxazole ring indicates that electropositive groups are favorable for activity. The red contours near carbonyl of amide group and the O atom in the isoxazole ring suggest that the electronegative groups are favorable to the activity. A blue contour and a red contour which are closer to ring D demonstrate that electronegative and electropositive groups at this position exerted similar influence on the inhibitory potency. In compounds 94(E) and 25(B), an electropositive group is seen in ring D. The substituted group of ring D in compound 16d(A) is an electronegative group and in compound 19d(D), are electropositive groups. The inhibitory activity of these compounds are the same, but in compound 3d(A) no electropositive group is seen in the region of rings D and C.

It can be realized that the steric and electrostatic contour map of CoMSIA and CoMFA are similar. According to the template displayed in the maps, CoMSIA steric and electrostatic contour (Figure 5(b) and (d)) present favorable and unfavorable areas which are comparatively similar to the map obtained from the CoMFA analysis mentioned above, and thus are not discussed here.

As seen in Figure 4, in the CoMSIA model, the hydrogen bond donor (HBD) field plays an important role in bioactivity than other CoMSIA fields. The cyan color contour denotes the HBD favorable region and the purple color contour denotes the HBD unfavorable region. As shown in Figure 6(a), presence of HBD favorable cyan contour near the NH group of amide moiety indicates that HBD group at this position is suitable for activity and the NH group at this position acted as a HBD. The HBD unfavorable purple contour was observed near the hydroxyl group of the resorcinol ring,

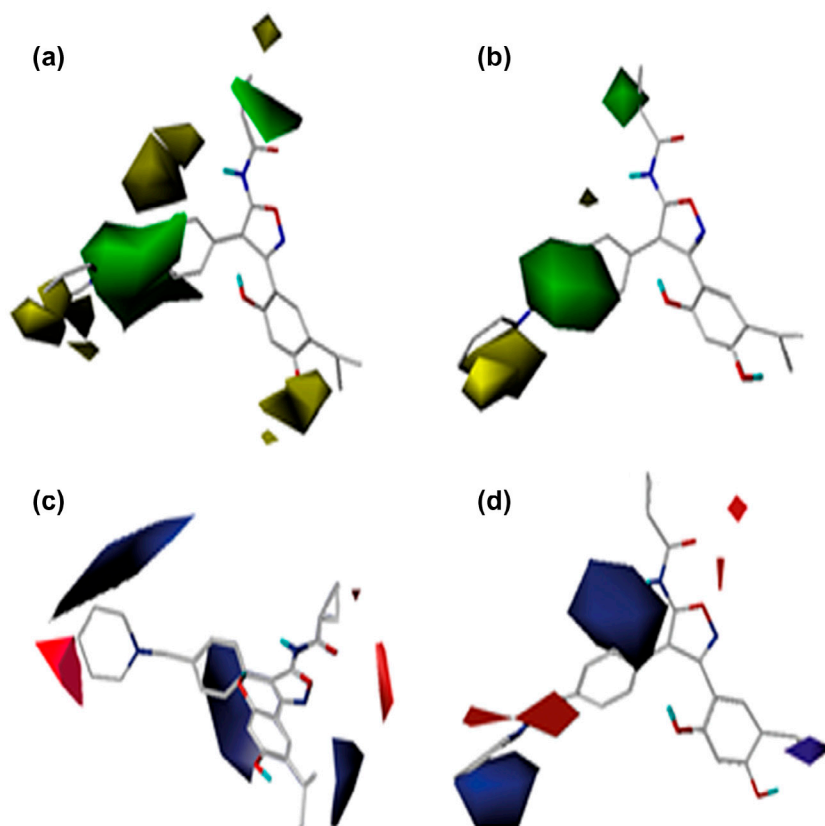


Figure 5. CoMFA and CoMSIA contour maps displayed using the most potent compound 94 (E) (a) CoMFA steric contour map (b) CoMSIA steric contour map; favored (green) and disfavored (yellow) (c) CoMFA electrostatic contour map (d) CoMSIA electrostatic contour map; electropositive (blue) and electronegative (red).

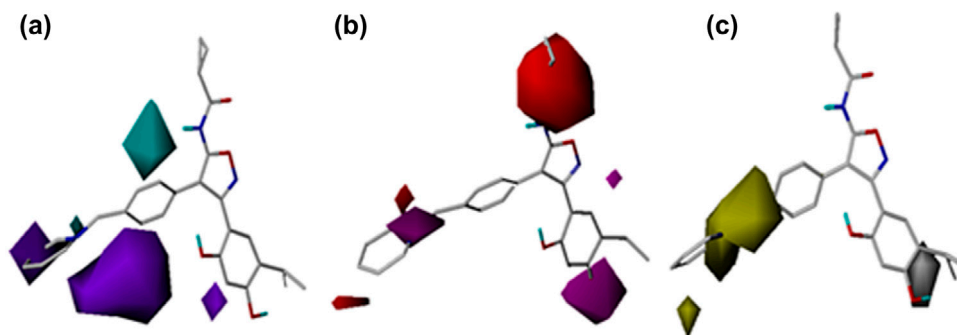


Figure 6. Contour maps of CoMSIA based on compound 94 (E); (a) Hydrogen bond donor field: the cyan color represents the favored H-donor region, and the purple color represents the disfavored H-donor region; (b) HBA field: the magenta color shows the favored H-acceptor region, the red color shows the disfavored H-acceptor region; (c) Hydrophobic field: the yellow color represents the favored hydrophobic region; the white color shows the disfavored hydrophobic region.

indicating that HBD group is not favorable at this position. The two large HBD unfavorable purple contours and a small HBD favorable cyan contour around

ring D imply that the HBD group is not favorable at this position. According to Figure 6(b), in the CoMSIA hydrogen bond acceptor (HBA) contour map, the

magenta color contour demonstrates the HBA favorable region and red color contour demonstrates the HBA unfavorable region. The magenta and red color contour around ring D shows that HBA group is not important in this region. The HBA unfavorable red contour was observed near the CO group of the amide, demonstrating that the HBA group is not favorable at this position. The magenta color contour near the isoxazole ring and the hydroxyl group of the resorcinol ring indicate that the HBA groups are preferred here.

In the CoMSIA hydrophobic contour maps, the white-colored contour shows regions where hydrophobic substitutions were unfavorable and the yellow-colored contour shows regions where the hydrophobic substitutions were favorable (Figure 6(c)). A large hydrophobic favored yellow contour was found between phenyl and piperidine rings, suggesting that a hydrophobic group at this position would be favorable for activity. Moreover, the hydrophobic unfavorable (hydrophilic favorable) white contour was seen near the hydroxyl group of the resorcinol ring, indicating the importance of hydrophilic moiety. In compound 3d(A), no hydrophobic or HBD groups were observed and only one acceptor group was seen in this compound, making it the compound with lowest activity. However, in compounds 25(B) and 19d (D), a hydrophobic group was seen around ring D, an HBD around the hydroxyl group of the resorcinol ring, and a HBA adjacent the carbonyl group of the amide.

#### Application domain of the model

The predicted compounds by a QSAR model are used when they entities falling within the applicability

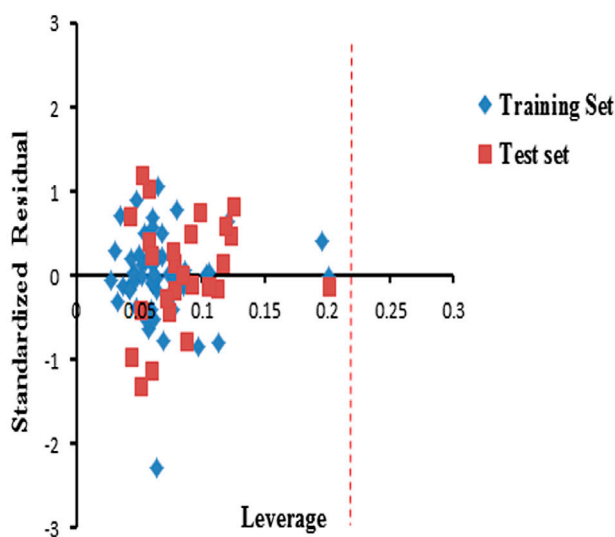


Figure 7. William's plot of generated CoMSIA model.

domain. Various approaches exist to determine application domain. Among the existing methods, the leverage approach (Williams plot) has been widely used to recognize the outliers (Roy, Kar, & Ambure, 2015). The leverage method is one of the distance-based methods which evaluate the distance of a compound from the testable space of model. The leverage value ( $h$ ) of predicted compounds must be lower than  $h^*$  ( $h^*$  is a threshold value equal to  $3(k+1)/n$ , where  $k$  is the number of model descriptors and  $n$  is number of the training set). Standardized residuals of the activity were calculated. The values of leverage and standardized residuals are always between 0–1 and  $\pm 3$ , respectively. A compound with values higher than 1 and  $\pm 3$  is outlier. The William's plot for the created CoMSIA model is shown in Figure 7 (Gadaleta, Mangiatordi, Catto, Carotti, & Nicolotti, 2016). As shown in Figure 7, most of the studied molecules in training and test set lie with high degree of confidence in application domain.

#### Propose of new compounds

According to CoMFA and CoMSIA contour maps that are shown in Figures 5 and 6, 12 novel inhibitors were proposed.

Regarding the point that bulky group and hydrophobic substitutions were seen unfavorable in resorcinol ring, the isopropyl group was removed in all the predicted compounds. Also in this region, HBA group is more important than HBD, so hydroxyl groups were converted to methoxy groups. In B and D rings area, medium-sized and hydrophobic groups are favorite groups, hence these rings displaced to four new groups. In E ring region, bulky and HBD groups are preferred. Eventually, in amide carbonyl moiety, only electronegative groups are favorable to the activity, so carbonyl group was eliminated and the electronegative group in ring E was substituted (Figure 8).

The first, validation docking on Hsp90 protein and the ligand in X-ray crystallography (3OWD) was done. The binding pocket in Hsp90N-terminal included hydrophobic and hydrophilic moieties and structural water molecules. The main residues in this pocket were Ala55, Ile96, Met98, Leu107, Phe138, Val150, Asn51, Asp93, and Thr184. Figure 9(a) shows hydrogen bonds between ligand (co-crystalized ligand; N-Aryl-benzimidazolone) and Asp93, Thr184 and the crystallographic water molecules. Also, the binding energy was calculated  $-4.93$  kcal/mol. The cluster analysis was performed with a tolerance at less than  $2 \text{ \AA}$  in positional root-mean-square deviation (RMSD). Afterward, docking studies were done on all predicted compounds. The docking results were shown in Table 3. All of compounds were perfectly placed

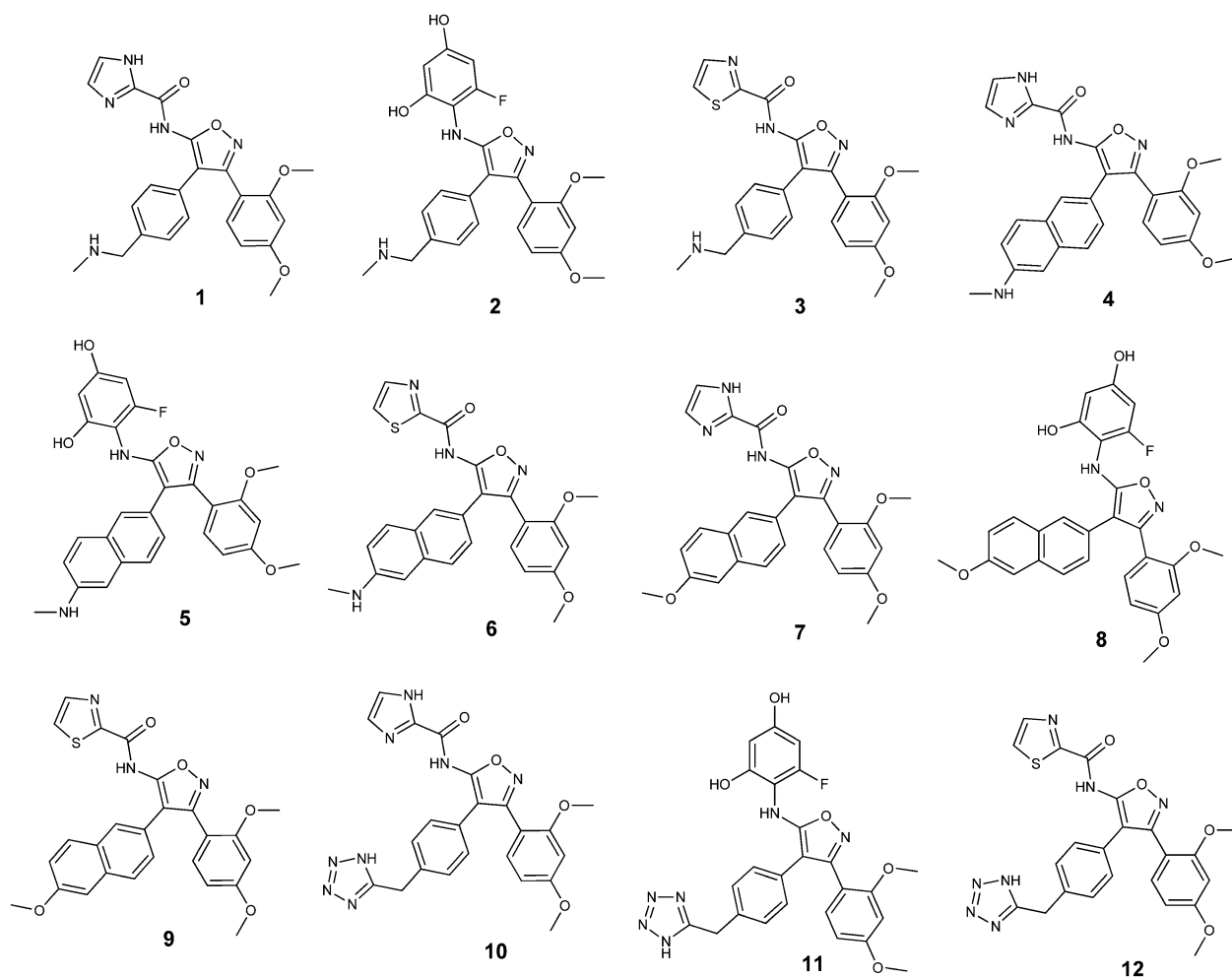


Figure 8. Chemical structures of 12 predicted compounds.

in the active site but compounds 1, 4, 5, 7, 8, 9, and 11 formed hydrogen bonds with Asp93, Thr184, and the crystallographic water molecules. Among the seven mentioned compounds, 1 demonstrated the lowest binding energy, so was chosen for more studies (Figure 9(b)).

To confirm the stability of compound 1 in the active site of Hsp90 protein, the MD simulation was performed and also to compare its interaction modes with that of compound 94(E) as the best inhibitor. In terms of the best orientation of the compound in the active site and the lowest binding energy, the best conformation of docking was chosen to run MD simulations. After 50 ns simulations, the time-dependent behavior of MD trajectories was analyzed.

To assess the conformational stability of Hsp90 during the simulation, RMSD of backbone atoms was calculated. As shown in Figure 10(a), the RMSD profile in Hsp90-compound 94(E) and Hsp90-predicted 1

complexes was perfectly superimposed in the first 25 ns and was almost the same in the last 10 ns. RMSD did not vary more than 0.3 nm in both complexes during the simulation, which suggests that both complexes were stable under the given simulation conditions. By studying the RMSD plots of the two ligands (Figure 10(b)), it can be detected that both of the ligands were stable after 8 ns and also fit in the active site and stabilized.

Gyration radius ( $R_g$ ), representing the compactness of the protein, was measured. In the first 35 ns, the  $R_g$  values of both complexes were superimposed, and in the last 15 ns they were nearly the same. Continuity of protein was maintained during the simulation in both complexes, as depicted in Figure 11. The root mean square fluctuation (RMSF) of backbone residues was carried out to recognize the variations of protein flexibility. As shown in Figure 12, the fluctuations in both complexes were almost the same. The residues 86–95, 146–164, and 170–188

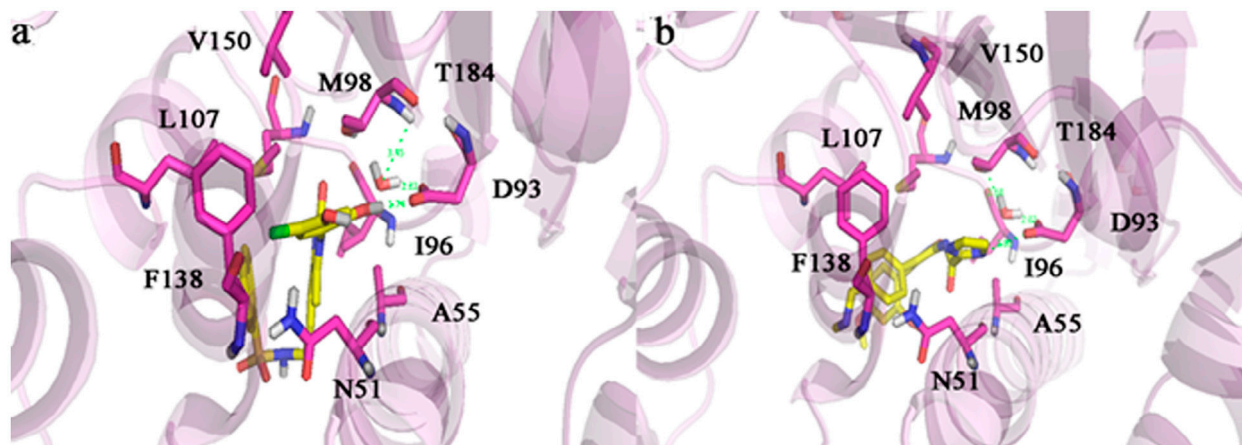


Figure 9. (a) Residues involved in the interaction of the ligand and Hsp90 in X-ray crystallography. (b) Residues involved in the interaction of the predicted compound 1 with Hsp90.

Table 3. Interactions between the docked predict compounds and Hsp90 binding site residues.

Predicted compounds	$\Delta G_{\text{binding}}$ (kcal/mol)	Hydrophilic amino acids	Hydrophobic amino acids
1	-6.42	Asp93, Asp54, Met98, Leu107	Thr184, Asn51, Ala55, Asn106, Ser52
2	-6.17	HOH, Ile110, Val136	Asp93, Thr184, Met98, Phe138, Asn51, Asn106, Leu107
3	-3.27	Asn51, HOH	Asp93, Thr184, Ala55, Met98, Phe138, Leu107, Ser52
4	-3.28	Asp93, Lys58, Asn106	Thr184, Met98, Asn51, Ala55, Leu107, Asp54
5	-3.26	Asp93, Asn51, Asn106	Ala55, Met98, Thr184, Leu107
6	-3.73	Asn106, Lys58	Asp93, Thr184, ASn51, Phe138, Leu107, Met98
7	-2.95	Asp93, Met98	Thr184, Ala55, Ser52, Asn51, Asn106, Leu107, Gly97
8	-3.42	Asp93, HOH	Thr184, Ser52, Ala55, Asn51, Phe138, Met98, Leu107, Asn106
9	-3.80	Asp93	Thr184, Ala55, Ser52, Asn51, Phe138, Asn106, Leu107, Met98, Ile96
10	-3.92	Asn51, Leu107, Lys58, HOH	Asp93, Thr184, Ala55, Asn106, Ile96
11	-4.49	Asp93, HOH	Thr184, Ala55, Asn51, Asn106, Met98
12	-4.52	Asn51, Gly135, HOH	Asp93, Thr184, Ala55, Ser52, Phe138, Leu107, Met98

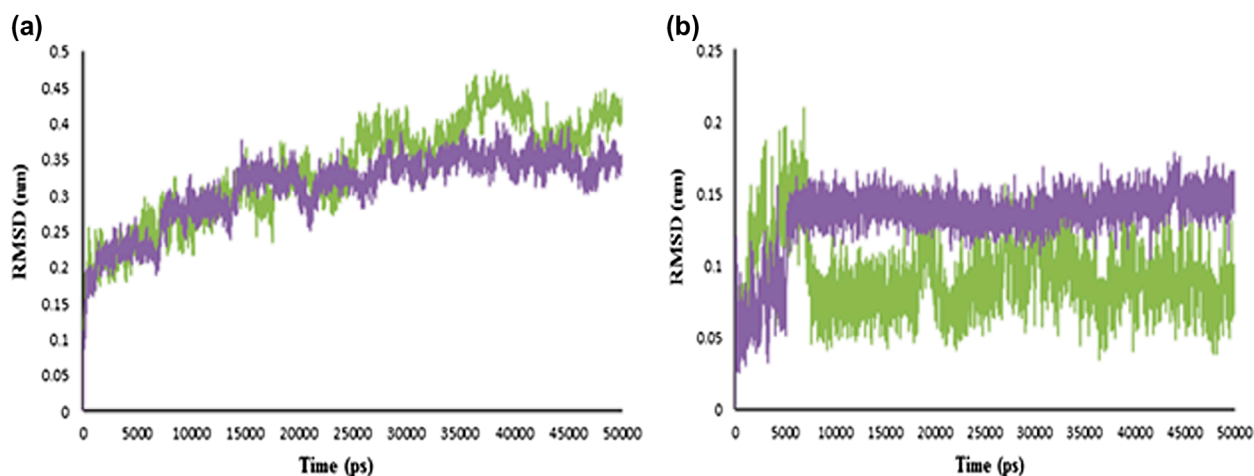


Figure 10. The RMSD profile. (a) Hsp90 backbone in complex with compound 94 (E) (violet), predicted compound 1 (green); (b) Compound 94 (E) (violet), predicted compound 1 (green) as a function of simulation.

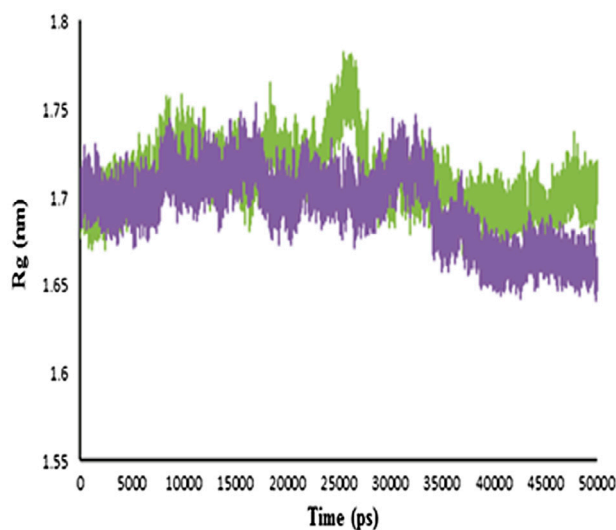


Figure 11. The gyration radius plot of backbone.Hsp90-compound 94 (E) (violet) and Hsp90-predicted compound 1 (green).

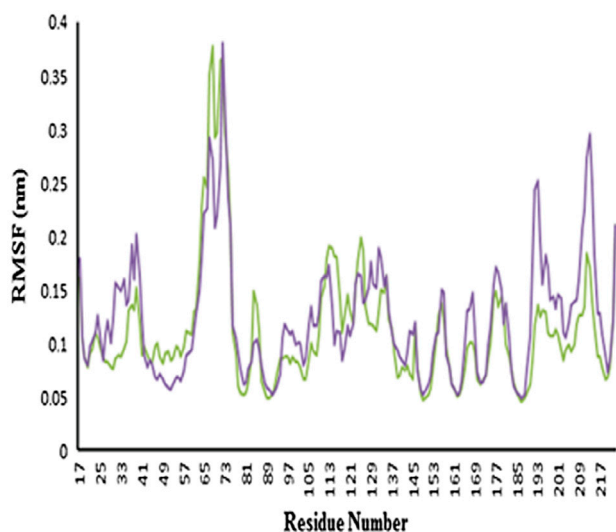


Figure 12. The RMSF plot of Hsp90-compound 94 (E) (violet) and Hsp90-predicted compound 1 (green).

were superimposed in both complexes. This indicates that these important regions (Asp93, Thr184, and Val150) had similar stability. In residues 95–110, the fluctuation of compound 94(E) was higher than that of predicted for 1, which reveals that the predicted compound was more stable than 94(E) in this part during the MD simulation. This is while in residues 44–71, compound 94(E) was more stable than the predicted compound. The MD

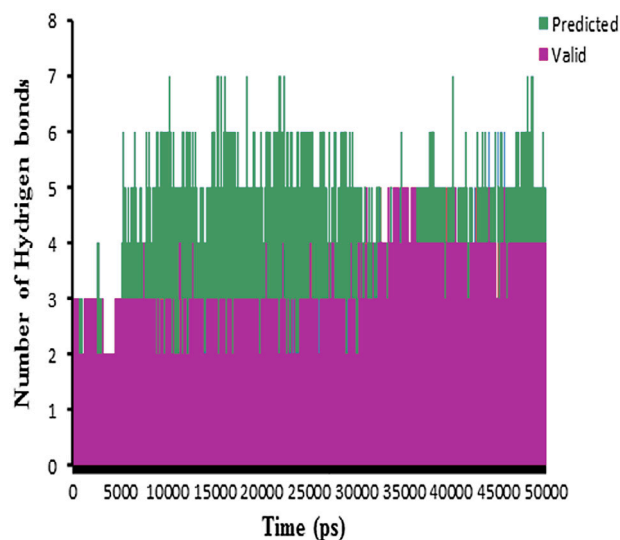


Figure 13. Number of H-bonds formed between Hsp90-compound 94 (E) (violet) and Hsp90-predicted compound 1 (green) during 50,000 ps MD simulation.

trajectories also were analyzed to calculate that number of hydrogen bonds (H-bonds) which were formed during MD simulation. Figure 13 shows fluctuation of number of H-bonds between 0 and 5 for compound 94(E)-Hsp90 and 0 and 7 for compound 1-Hsp90.

To compare the conformations and interactions of compound 94(E) and predicted ligand 1, 3D structures of different times of simulation 0, 25, and 50 ns are illustrated in Figure 14. At the beginning of simulation (0 ns), a hydrogen bond was formed between the O atom of the amide group and Thr184, with a distance of 3.59 Å in the predicted ligand, whereas in compound 94(E), the hydroxyl groups of the resorcinol ring made hydrogen bonds with Asp93 (3.82 and 1.89 Å distances). In both complexes, the residues Asn51, Ala55, I96, Met98, Asp93, Phe138, and Thr184 perched around the ligands. During the first 25 ns, in addition to the interaction between the ligand and Thr184, another hydrogen bond was created between the N atom of imidazole and Asp93 in the predicted ligand. The ligand was close to the main residues of protein, at a distance of 1.89 and 1.79 Å with Asp93 and Thr184, respectively. The orientation changed in compound 94(E). Two hydrogen bonds were seen between the O atom of amide group with Thr184 (1.80 Å distance) and the hydroxyl group of the resorcinol ring with Asp93 (A distance of 2.04 Å). Finally, at the end of the simulation (50 ns), both of the compounds were stable in the active site of the protein with hydrogen bonds and hydrophobic interactions and did not transfer outside of the active site during the simulation.

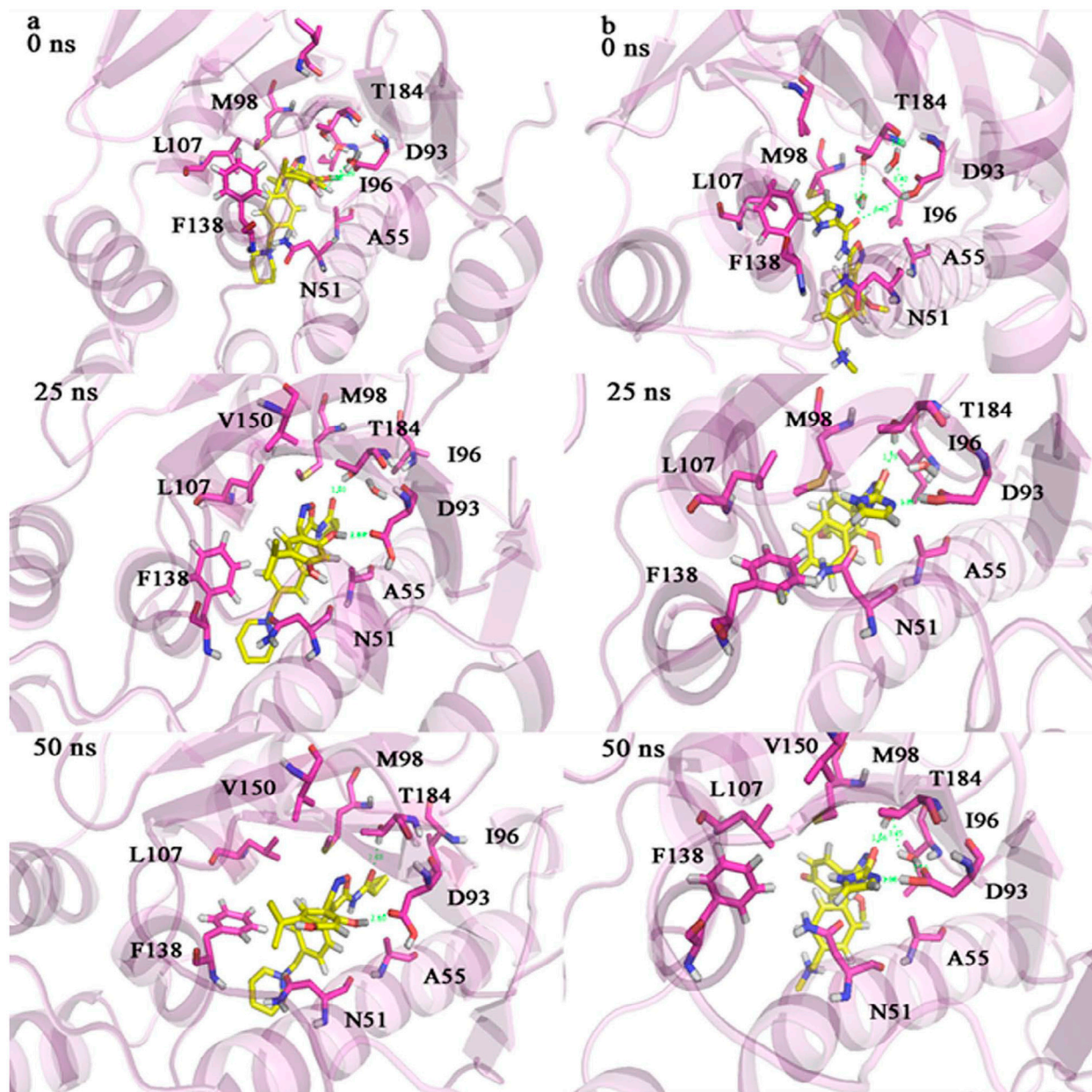


Figure 14. 3D plots of the interaction between two ligands and Hsp90 at different times during the MD simulation. (Column a) The interaction of compound 94 (E) with Hsp90. (Column b) The interaction of the predicted compound with Hsp90.

## Conclusion

A ligand-based pharmacophore (3D-QSAR) study was carried out in combination with structure-based molecular modeling and MD simulation to propose new inhibitors of Hsp90. The pharmacophore-based alignment of isoxazole ring was exercised to develop significant 3D-QSAR for propose 3D features that influences biological activity. Among seven created contour maps from CoMFA and CoMSIA analyses, HBD was the most effective. According to 3D-QSAR pharmacophore, 12

compounds were proposed. The binding modes of the proposed compounds at the active site of Hsp90 protein were recognized by molecular docking. All compounds were perfectly placed in the active site and seven compounds formed hydrogen bonds with Asp93, Thr184, and the crystallographic water molecules. To confirm the stability of the predicted compounds in the active site of Hsp90 protein, a MD simulation was done on one of them. MD simulation analyses on predicted compound such as RMSD, RMSF, and Rg revealed that predicted

compound is stable in Hsp90 active sites. Therefore, 3D-QSAR can be used as a powerful tool to predict new Hsp90 inhibitors, based on isoxazole backbone.

### Abbreviations

Hsp90	heat shock protein90
ATP	adenosine triphosphate
3D-QSAR	three-dimensional quantitative structure–activity relationship
MDs	molecular dynamic simulation
PLS	partial least squares
$Q_{LOO}^2$	square correlation coefficient for leave-one-out cross-validation
$R^2$	calibration correlation coefficient
SE	standard error of calibration
RMSD	root-mean-square deviation
RMSF	root-mean-square fluctuation
Rg	gyration radius

### Disclosure statement

No potential conflict of interest was reported by the authors.

### Funding

This work was supported by the Tehran University of Medical Sciences and Health Services [grant number TUMS-15865].

### References

- Abbasi, M., Ramezani, F., Elyasi, M., Sadeghi-Aliabadi, H., & Amanlou, M. (2015). A study on quantitative structure–activity relationship and molecular docking of metalloproteinase inhibitors based on L-tyrosine scaffold. *DARU Journal of Pharmaceutical Sciences*, 23, 1–10.
- Abbasi, M., Sadeghi-Aliabadi, H., Hassanzadeh, F., & Amanlou, M. (2015). Prediction of dual agents as an activator of mutant p53 and inhibitor of Hsp90 by docking, molecular dynamic simulation and virtual screening. *Journal of Molecular Graphics and Modelling*, 61, 186–195.
- Abraham, M. J., Murtola, T., Schulz, R., Páll, S., Smith, J. C., Hess, B., & Lindahl, E. (2015). GROMACS: High performance molecular simulations through multi-level parallelism from laptops to supercomputers. *SoftwareX*, 1–2, 19–25.
- Athar, M., Lone, M. Y., Khedkar, V. M., & Jha, P. C. (2016). Pharmacophore model prediction, 3D-QSAR and molecular docking studies on vinyl sulfones targeting Nrf2-mediated gene transcription intended for anti-Parkinson drug design. *Journal of Biomolecular Structure and Dynamics*, 34, 1282–1297.
- Azizian, H., Bahrami, H., Pasalar, P., & Amanlou, M. (2010). Molecular modeling of *Helicobacter pylori* arginase and the inhibitor coordination interactions. *Journal of Molecular Graphics and Modelling*, 28, 626–635.
- Bargiotti, A., Musso, L., Dallavalle, S., Merlini, L., Gallo, G., Ciacci, A., ... Vesce, L. (2012). Isoxazolo(aza)naphthoquinones: A new class of cytotoxic Hsp90 inhibitors. *European Journal of Medicinal Chemistry*, 53, 64–75.
- Baruchello, R., Simoni, D., Grisolia, G., Barbato, G., Marchetti, P., Rondanin, R., ... Alloatti, D. (2011). Novel 3,4-isoxazolidiamides as potent inhibitors of chaperone heat shock protein 90. *Journal of Medicinal Chemistry*, 54, 8592–8604.
- Baruchello, R., Simoni, D., Marchetti, P., Rondanin, R., Mangiola, S., Costantini, C., ... Carollo, V. (2014). 4, 5, 6, 7-Tetrahydro-isoxazolo-[4, 5-c]-pyridines as a new class of cytotoxic Hsp90 inhibitors. *European Journal of Medicinal Chemistry*, 76, 53–60.
- Bringmann, G., & Rummey, C. (2003). 3D QSAR investigations on antimalarial naphthylisoquinoline alkaloids by comparative molecular similarity indices analysis (CoMSIA), based on different alignment approaches. *Journal of Chemical Information and Computer Sciences*, 43, 304–316.
- Bruncko, M., Tahir, S. K., Song, X., Chen, J., Ding, H., Huth, J. R., ... Park, C. H. (2010). N-Aryl-benzimidazolones as novel small molecule HSP90 inhibitors. *Bioorganic & Medicinal Chemistry Letters*, 20, 7503–7506.
- Chauhan, J. S., Dhanda, S. K., Singla, D., Agarwal, S. M., Raghava, G. P., & Consortium, O. S. D. D. (2014). QSAR-based models for designing quinazoline/imidazothiazoles/pyrazolopyrimidines based inhibitors against wild and mutant EGFR. *PLoS ONE*, 9, e101079.
- Chen, D., Shen, A., Li, J., Shi, F., Chen, W., Ren, J., ... Yang, X. (2014). Discovery of potent N-(isoxazol-5-yl)amides as HSP90 inhibitors. *European Journal of Medicinal Chemistry*, 87, 765–781.
- Cosconati, S., Forli, S., Perryman, A. L., Harris, R., Goodsell, D. S., & Olson, A. J. (2010). Virtual screening with AutoDock: Theory and practice. *Expert Opinion on Drug Discovery*, 5, 597–607.
- Cramer, R. D., Bunce, J. D., Patterson, D. E., & Frank, I. E. (1988). Crossvalidation, bootstrapping, and partial least squares compared with multiple regression in conventional QSAR studies. *Quantitative Structure-Activity Relationships*, 7, 18–25.
- Frisch, M. (1998). *Gaussian98, revision A. 7*. Pittsburgh, PA: Gaussian, Inc.
- Frisch, M. J., Trucks, G. W., Schlegel, H. B., & Scuseria, G. E. (2004). *Gaussian03, revision C. 01*. Wallingford, CT: Gaussian, Inc.
- Gadaleta, D., Mangiatordi, G. F., Catto, M., Carotti, A., & Nicolotti, O. (2016). Applicability domain for QSAR models. *International Journal of Quantitative Structure-Property Relationships*, 1, 45–63.
- Humphrey, W., Dalke, A., & Schulten, K. (1996). VMD: Visual molecular dynamics. *Journal of Molecular Graphics*, 14, 33–38.
- Klebe, G., Abraham, U., & Mietzner, T. (1994). Molecular similarity indices in a comparative analysis (CoMSIA) of drug molecules to correlate and predict their biological activity. *Journal of Medicinal Chemistry*, 37, 4130–4146.
- Ma, S., Zeng, G., Fang, D., Wang, J., Wu, W., Xie, W., ... Zheng, K. (2015). Studies of N 9-arethenyl purines as novel DFG-in and DFG-out dual Src/Abl inhibitors using 3D-QSAR, docking and molecular dynamics simulations. *Molecular BioSystems*, 11, 394–406.
- Makarewicz, T., & Kaźmierkiewicz, R. (2013). Molecular dynamics simulation by GROMACS using GUI plugin for PyMOL. *Journal of Chemical Information and Modeling*, 53, 1229–1234.
- McLaughlin, S. H., Sobott, F., Yao, Z.-P., Zhang, W., Nielsen, P. R., Grossmann, J. G., ... Jackson, S. E. (2006). The co-



- chaperone p23 arrests the Hsp90 ATPase cycle to trap client proteins. *Journal of Molecular Biology*, 356, 746–758.
- Morris, G. M., Goodsell, D. S., Halliday, R. S., Huey, R., Hart, W. E., Belew, R. K., & Olson, A. J. (1998). Automated docking using a Lamarckian genetic algorithm and an empirical binding free energy function. *Journal of Computational Chemistry*, 19, 1639–1662.
- Morris, G. M., Huey, R., Lindstrom, W., Sanner, M. F., Belew, R. K., Goodsell, D. S., & Olson, A. J. (2009). AutoDock4 and AutoDockTools4: Automated docking with selective receptor flexibility. *Journal of Computational Chemistry*, 30, 2785–2791.
- Musso, L., Cincinelli, R., Giannini, G., Manetti, F., & Dallavalle, S. (2015). Synthesis of 5, 6-dihydro-4H-benzo [d] isoxazol-7-one and 5, 6-dihydro-4H-isoxazolo [5, 4-c] pyridin-7-one Derivatives as Potential Hsp90 Inhibitors. *Chemical Biology & Drug Design*, 86, 1030–1035.
- Ouyang, L., He, G., Huang, W., Song, X., Wu, F., & Xiang, M. (2012). Combined structure-based pharmacophore and 3D-QSAR studies on phenylalanine series compounds as TPPI inhibitors. *International Journal of Molecular Sciences*, 13, 5348–5363.
- Porter, J. R., Fritz, C. C., & Depew, K. M. (2010). Discovery and development of Hsp90 inhibitors: A promising pathway for cancer therapy. *Current Opinion in Chemical Biology*, 14, 412–420.
- Pourbasheer, E., Bazl, R., & Amanlou, M. (2014). Molecular docking and 3D-QSAR studies on the MAPKAP-K2 inhibitors. *Medicinal Chemistry Research*, 23, 2252–2263.
- PyMOL. (2010). *The PyMOL molecular graphics system: Version*. San Carlos, CA: DeLano Scientific.
- Roy, K., Kar, S., & Ambure, P. (2015). On a simple approach for determining applicability domain of QSAR models. *Chemometrics and Intelligent Laboratory Systems*, 145, 22–29.
- Roy, K., Kar, S., & Das, R. N. (2015). *Understanding the basics of QSAR for applications in pharmaceutical sciences and risk assessment*. New York: Academic Press.
- Schmid, N., Eichenberger, A. P., Choutko, A., Riniker, S., Winger, M., Mark, A. E., & van Gunsteren, W. F. (2011). Definition and testing of the GROMOS force-field versions 54A7 and 54B7. *European Biophysics Journal*, 40, 843–856.
- Schüttelkopf, A. W., & van Aalten, D. M. (2004). PRODRG: A tool for high-throughput crystallography of protein–ligand complexes. *Acta Crystallographica Section D: Biological Crystallography*, 60, 1355–1363.
- Sharma, S. V., Agatsuma, T., & Nakano, H. (1998). Targeting of the protein chaperone, HSP90, by the transformation suppressing agent, radicicol. *Oncogene*, 16, 2639–2645.
- Sharp, S. Y., Prodromou, C., Boxall, K., Powers, M. V., Holmes, J. L., Box, G., ... James, K. (2007). Inhibition of the heat shock protein 90 molecular chaperone in vitro and in vivo by novel, synthetic, potent resorcinolic pyrazole/isoxazole amide analogues. *Molecular Cancer Therapeutics*, 6, 1198–1211.
- Søndergaard, C. R., Olsson, M. H., Rostkowski, M., & Jensen, J. H. (2011). Improved treatment of ligands and coupling effects in empirical calculation and rationalization of p K a values. *Journal of Chemical Theory and Computation*, 7, 2284–2295.
- Sun, J., Lin, C., Qin, X., Dong, X., Tu, Z., Tang, F., ... Zhang, J. (2015). Synthesis and biological evaluation of 3, 5-disubstituted-4-alkynylisoxozales as a novel class of HSP90 inhibitors. *Bioorganic & Medicinal Chemistry Letters*, 25, 3129–3134.
- Tripuraneni, N. S., & Azam, M. A. (2016). A combination of pharmacophore modeling, atom-based 3D-QSAR, molecular docking and molecular dynamics simulation studies on PDE4 enzyme inhibitors. *Journal of Biomolecular Structure and Dynamics*, 34, 2481–2492.
- Wandinger, S. K., Richter, K., & Buchner, J. (2008). The Hsp90 chaperone machinery. *Journal of Biological Chemistry*, 283, 18473–18477.
- Yang, Y., Wang, J., Li, Y., Xiao, W., Wang, Z., Zhang, J., ... Yang, L. (2013). Structure determinants of indolin-2-on-3-spirothiazolidinones as MptpB inhibitors: An in silico study. *Soft Matter*, 9, 11054–11077.
- Zhou, S., Fang, D., Tan, S., Lin, W., Wu, W., & Zheng, K. (2016). Investigating the binding mechanism of novel 6-aminonicotinate-based antagonists with P2Y12 by 3D-QSAR, docking and molecular dynamics simulations. *Journal of Biomolecular Structure and Dynamics*, 1–28.